HADES — A HIGH ACCEPTANCE DIELECTRON SPECTROMETER*

P. SALABURA

Institute of Physics, Jagellonian University
Reymonta 4, 30-059 Cracow, Poland

FOR THE HADES COLLABORATION**

(Received December 8, 1995)

A High Acceptance DiElectron Spectrometer (HADES) has been proposed at the SIS accelerator of GSI in order to measure e^+e^- pairs produced in proton, pion and heavy ion induced reactions. HADES will be able to operate at the highest luminosities available at SIS in an environment of high hadron and photon background. A Ring Imaging Čerenkov Counter (RICH) serves for electron identification. Momentum measurement is achieved with a magnetic spectrometer consisting of superconducting toroidal coils and mini drift chambers for tracking. Arrays of pre-shower detectors and a Time Of Flight wall are positioned behind the drift chambers for electron trigger purposes and for measuring the charged particle multiplicity. The detector features have been investigated in detailed simulations. The expected performance of the system in terms of efficiency, resolution and residual background is presented. First results from prototype tests of HADES detectors are briefly discussed.

PACS numbers: 25.75.-q

Introduction

HADES is a second-generation apparatus currently under design and construction at GSI Darmstadt. The physics program of HADES is devoted to investigate the in-medium properties of the light vector mesons

* Presented at the XXIV Mazurian Lakes School of Physics, Piaski, Poland, August 23–September 2, 1995.

** IOP Bratislava, Univ. Clermont-Ferrand, Univ. Frankfurt, Univ. Giessen, GSI Darmstadt, Jagellonian Univ. Cracow, ITEP Moscow, LPI Moscow, MEPI Moscow, TU Munich, Univ. Nikosia, INP Rez, Univ. Valencia

like $\rho(770\ \mathrm{MeV/c^2})$, $\omega(783\ \mathrm{MeV/c^2})$ and $\phi(1020\ \mathrm{MeV/c^2})$ in pp-, pA- and AA-collisions as well as in π induced reactions. One of the aims of these studies is to explore in-medium modifications of hadron properties, such as the mass shifts or width changes, as predicted by various model calculations [2, 4–7]. In particular, the ρ meson focused a lot of interest since its short life time (roughly 1 fm/c) results in a decay inside the hadron matter. Medium modifications should lead to significant effects in the measured dilepton invariant mass spectrum [1, 2, 8]. The comparison of pA- and AA-collisions allows to study these effects as a function of hadronic matter density. Moreover, a program for the investigation of meson and baryon electromagnetic form factors is planned, which will exploit the future availability of pion beams at GSI. Detailed theoretical discussion of in-medium modifications and electromagnetic form factors of mesons is given in Soyeur's contribution to this conference.

Due to the electromagnetic coupling the dielectron decay channel of vector mesons is suppressed by a factor of $\approx 10^{-5}$ as compared to the hadronic decay channels. Together with the small subthreshold production cross sections the expected total yield of dielectrons from vector mesons is only of the order of 10^{-6} per central Au+Au collision at 1 AGeV [9]. Thus the experimental challenge is to find one dielectron in one million of these central collisions each containing about 400 hadrons and 25 photons from π^0-decay. This requires a system with large geometrical acceptance, high rate capabilities allowing operation at beam intensities of up to 10^8 particles/s currently available at GSI, sufficient granularity and a highly selective multi-stage trigger scheme. For the fast electron recognition the hadron blind detectors with on-line image processing are necessary. Moreover, an excellent invariant mass resolution is required for the identification of vector mesons.

What is the experimental information available up to know? The pioneering experiments at the BEVELAC [12] as well as the second generation experiments at GSI confirmed formation of dense nuclear matter in a course of heavy ion collisions at 1–2 AGeV. In particular, GSI data concerning fragmentation [23] or meson subthreshold production [11, 24] provides a nice experimental verification of this scenario. Dilepton production was studied by pioneering experiments of the DLS collaboration [10] carried out at the BEVELAC. They found evidence for contributions to the dielectron invariant mass spectrum from meson decay [21]. Nevertheless, in case of the heaviest system measured (Ca+Ca at 1 AGeV) the pure statistics and resolution did not allow to draw any conclusions on possible changes of width or mass of the ρ meson as compared to its vacuum properties. Recently, the CERES collaboration reported an exciting result. In 200 AGeV Si + Au collisions measured at CERN a large dilepton excess below rho-omega

region has been observed [13], when compared to properly scaled results for p + Be providing for the first time an evidence for a new source of dilepton production in relativistic heavy-ion collisions.

Design of the Spectrometer

The proposed device is a rotationally symmetric, large acceptance toroidal spectrometer. With this geometry, complete azimuthal coverage is achieved. The design values for the angular and momentum acceptance were chosen according to the two-body decay kinematics at SIS energies assuming thermal emission from a mid-rapidity ($Y = 0.6 - 0.85$) zone. These dielectrons are emitted over the whole polar angular range with a maximum probability at about 40°. HADES will cover polar angles from 18° to 85°. For masses up to 1.5 GeV/c^2 and transverse momenta up to 1.5 GeV/c this geometry results in a flat acceptance. The geometrical acceptance of ~40% represents an improvement by a factor of 100 as compared to the pioneering experiments performed with the DLS spectrometer at Berkeley [10, 14].

The proposed strategy for the measurement of dielectrons consist of: electron identification in the dedicated detectors before and behind magnetic field and momentum determination (Fig. 1):

- A first electron identification over the full acceptance is done by a fast RICH (Ring Imaging Čerenkov Counter) with gaseous radiator surrounding the target in the forward hemisphere. Selection of the gaseous radiator ensures a virtualy hadron blind detector as well as low multiple scattering of electron and allows for its precise reconstruction in the following tracking section.
- Momentum analysis is achieved by a trajectory reconstruction in the 2 sets of Mini-Drift Chambers (MDCs) positioned in 6 spectrometer sectors. A toroidal field geometry (6 superconducting coils) is the optimal choice for the following reasons: First, while covering the large forward solid angle, a field free region for the RICH can be achieved inside the toroid. This ensures detection of undisturbed Čerenkov rings and enables the rejection of low mass pairs. Second, the field geometry is well matched to the dielectron kinematics since the radial $1/r$ dependence of the field compensates for the fact that the mean electron momentum increases for decreasing polar angles.
- The first level trigger on central events is obtained from the multiplicity measurement performed by the scintillator wall surrounding the outer MDCs. For the beam intensities mentioned above and 1% interaction length target thickness, a mean first level trigger rate of $10^5 s^{-1}$ is expected. The other part of META (Multiplicity and Electron Trigger

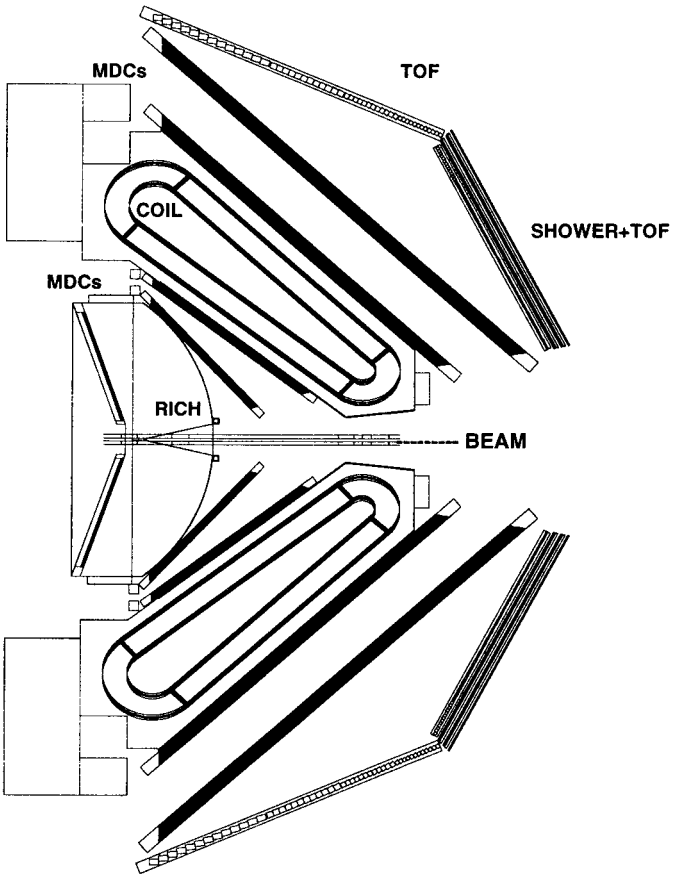

Fig. 1. Azimuthal cross section of the HADES setup. The RICH consists of a gaseous radiator, carbon fiber mirror and the tilted UV detector segments. The target is positioned in the center of the radiator. Two sets of mini-drift chambers (MDCs) in front and behind the magnetic field produced by superconducting coils measure the trajectory. A time of flight wall (TOF) is foreseen as a first level trigger and for second electron identification. At polar angles $< 45°$ the TOF wall is accompanied by a pre-shower detector.

Array) is the pre-shower detector, placed at smaller polar angles and used together with the TOF measurement serving for the second electron identification device. The aim of the second level trigger is to perform fast ($\leq 10\mu$s) electron identification in the dedicated RICH and META processors which are connected to the detector readouts. The identified positions of electron hits in RICH are then combined with identified electron hit positions in META in order to investigate their angular correlation.

The performance of the spectrometer was studied by detailed simulations using GEANT and including the complete geometry of the setup as well as realistic detector responses. The signal to background ratio has been investigated for various collision systems. Results for a most difficult case, central Au + Au collisions at $1A$GeV, are presented in the last section. In the following we describe the three main HADES components: RICH, Magnetic Spectrometer and META.

The RICH detector

The RICH is the main component for electron identification. It consists of a gaseous radiator surrounding the target in the forward hemisphere, spherical mirror and position sensitive photon detector (Fig. 2). The Čerenkov light from electrons emitted in a cone along their way through the radiator is reflected by a spherical aluminized carbon fiber mirror (radius 89.4 cm, thickness 0.2 cm) and focused onto a position sensitive photon detector. A gaseous radiator ensures a high velocity threshold for the Čerenkov effect. However, in order to obtain reasonable photon statistics the selection of a photon detector sensitive in the Ultra Violet (UV) region (note $1/\lambda^2$ dependence of the Čerenkov light intensity) requires as well as high UV mirror reflectivity as a good radiator gas transmission.

An UV reflectivity of the mirror of ~85% down to $\lambda = 140$ nm has been routinely obtained. To obtain a resolution of about 1mm for the determination of the ring centers variation of the mirror surface should not exeed $\delta = 30\mu$m for a typical electron Cherenkov ring of 5 cm diameter.

The flourocarbon based radiator gases C_2F_6 or C_4F_{10} are proposed for the following reasons:

1. The threshold value $\gamma_{th} = 22$ yields a sufficient number of Čerenkov photons. Nevertheless, hadron blindness for the given momentum range is achieved. All protons and practically all pions in the SIS energy range have velocities below the radiator threshold ($p^p_{th} \simeq 20$ GeV/c, $p^\pi_{th} \simeq 3.1$ GeV/c). For electrons the threshold amounts to $p^e_{th} \simeq 11.1$ MeV/c which is well below the HADES momentum region of interest.
2. The high UV transmission with a cutoff below 145 nm results in a high Čerenkov photon yield per unit path length. The radiator can therefore be built in a compact way.
3. From scintillation light measurements for C_2F_6 or C_4F_{10} and CH_4 [16] only a small number of scintillation photo electrons of ≤ 100 per/central Au + Au collision at $1A$GeV is estimated (single hits in Fig. 4).

To match the expected reaction rates of up to 10^6 s^{-1} the UV detector is designed as a fast Multi Wire Proportional Chamber (MWPC). The

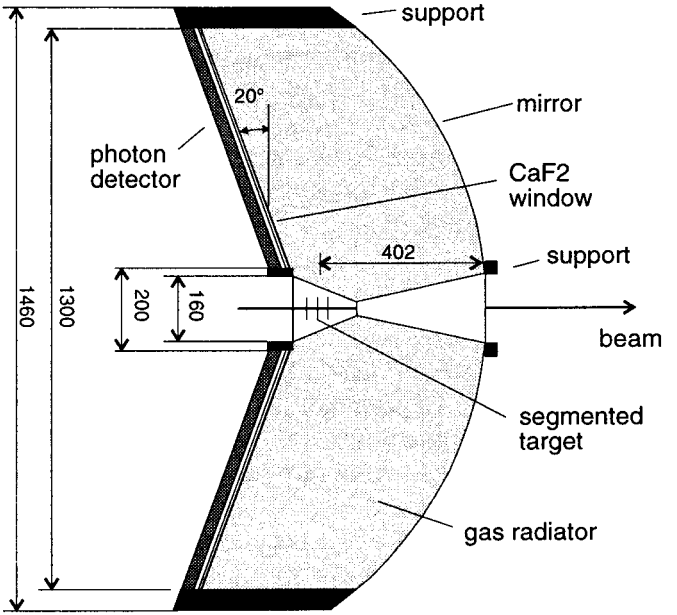

Fig. 2. Schematic view of the HADES Ring Imaging Čerenkov Counter (RICH): Electrons passing the radiator produce Čerenkov photons which are reflected by the aluminized carbon fiber mirror and focused towards the UV detector. The UV detector is a MWPC with a solid photocathode of evaporated CsI. Tilt angle and position of the UV detector are adapted to the shape of the focal plane.

UV detector consist of 6 identical MWPC modules filled with CH_4 and is equipped with a solid photocathode of evaporated CsI. It is separated from the radiator volume by an 8 mm CaF_2 window. A prototype of the photon detector with quartz entrance window and 48 x 48 cm^2 active area has been build and succesfully tested (Fig. 3) [18]. The detector, although rectangular, is similar in size to one segment of the HADES RICH. The solid photocathode is divided into 6×6 mm^2 pads spaced by 1.2 mm from the anode wire plane. The other cathode plane is a wire mesh of 1.5 pitch placed 2.6 mm above anode wires. The asymmetric field gap ensures reduced cross-talk between adjacent pads. The measured quantum efficiency of the photocathode increases with shorter wavelengths and reaches 45% at the radiator transmission cutoff of 140 nm [17]. The expected single photoelectron detection efficiency is about 90%. The ring quality is mainly determined by the focusing properties of the mirror due to an extended and curved focusing plane (spherical aberration). This results in elliptically deformed ring images. The 20° tilt angle of the six azimuthal UV detector segments is roughly matched to this focal plane. Moreover, in order to approximately correct eccentricity of the ring images and to simplify the

design of the trigger processor the pad shape of the final UV detector will be modified as a function of the polar angle.

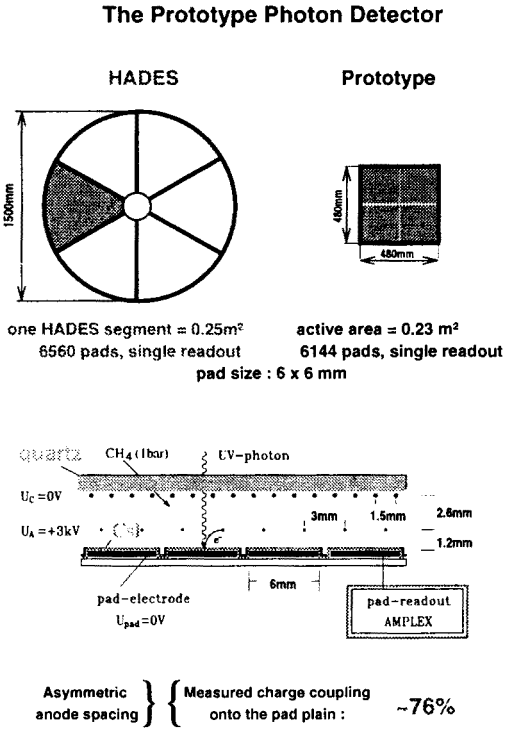

Fig. 3. Schematic view of the photo sensitive Multi Wire Proportional Chamber (MWPC) with a pad cathode covered by CsI. The full size photon detector consist out of six sectors with 6560 pad read out channels each. The prototype chamber of similar size but quadratic shape has been constructed and tested. Due to the asymmetric cathode-anode-pad plane spacing a reduction of the charge coupling on surrounding pads has been achieved

Within the range of lepton polar emission angles θ, corresponding to radiator lengths of 42–73 cm, an avarage number of 15–26 photons is detected per ring. These numbers have been simulated taking into account the given detection efficiency of the UV-detector, transmission losses in the radiator gas and the CaF_2 window as well the losses due to the mirror reflectivity (0.85). In 1–2 AGeV Au + Au collisions most of the Čerenkov rings are due to the π° decay products ($\pi^0 \rightarrow \gamma\gamma(\sim 99\%)$ and $\pi^0 \rightarrow \gamma e^+e^-(\sim 1\%)$) External Pair Creation (EPC) of γ-ray from π^0 decay in the segmented target and in the radiator contributes equally with ~ 0.2 pairs/collision. Only one ring is produced by such pairs due to the small mean pair opening angle of $\sim 0.5^\circ$. Dalitz pairs from π^0 decay (0.13 pairs/collision) have a larger

mean opening angle of 16° and produce partially overlapping rings. After rejecting pairs of rings with opening angles smaller than 15° the number of single background rings amounts to $\simeq 0.5$/central collision. Further rejection methods have to be applied (see below) since combinatorial background from Dalitz and EPC pairs results in an opening angle distribution similar to that of the two body decay of vector meson (mean opening angle 90°). Fig. 4 shows a typical RICH hit pattern as simulated for 1 AGeV Au + Au collisions. The two Čerenkov rings marked by circles are produced by an ω decay contained in this event.

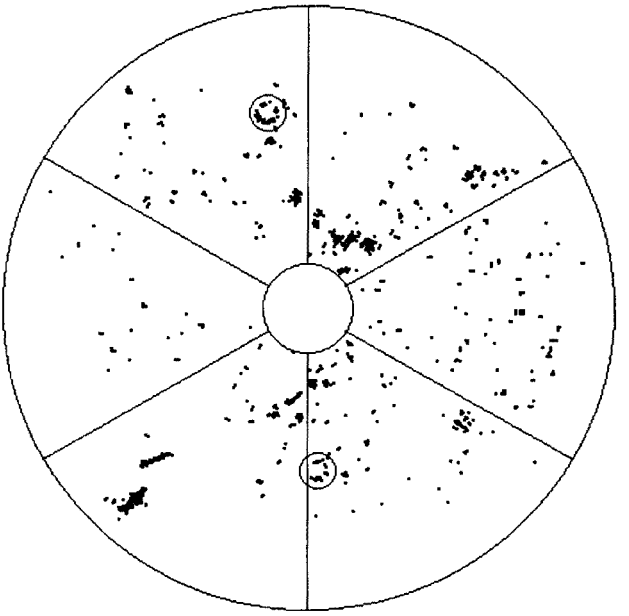

Fig. 4. RICH hit pattern for central Au + Au collisions at 1AGeV containing one e^+e^- pair from ω. The Čerenkov rings produced by the electrons are marked with circles. The clusters originate from ionisation of charged particles and from Čerenkov light produced in the CaF_2 window. Single hits are due to scintillation light and electronic noise.

The resulting total number of 6560 pads per sector has to be individually read-out and digitized within 10 μs to match the mean speed of the first level trigger. It is planned to use CERN-developed GASIPLEX or AMPLEX [19] 16 channel analog signal processing chips consisting of charge-sensitive amplifier, shaper and store and hold stage. These signals are multiplexed to one 8 bit flash-ADC and compared to the threshold. The bit-pattern of fired pads will be used in the RICH part of the second level trigger based on Fast Programmable Gate Arrays (FPGA) performing ring search.

The pulse height data, after zero suppression, are written to a local detector memory and are send to an event builder after a positive second level trigger decision. For central Au + Au at 1AGeV collisions 400 active pads per event are expected.

For the prototype UV detector all 6144 pads have already been equipped with the read-out electronics as described above. The detector has been successfully operated in a test experiment at GSI [18]. The results of this measurement are presented below.

UV detector prototype results

The test experiment was performed at GSI Darmstadt to detect Cherenkov photons produced by $E_{\mathrm{kin}} = 413$ AMeV ^{12}C-ions passing a $l_{\mathrm{rad}} = 2$ mm thick MgF_2 radiator. The parameters were chosen such that intensities and radii of the Cherenkov rings were similar of those expected in the HADES RICH. The setup is schematically shown in Fig. 5. The measured Cherenkov ring integrated over several events is shown together with its radial distribution in Fig. 5. The latter one is calculated with respect to the ring centers deduced from the direction of tracks of impinging ions. The expected radial distribution is shown for comparison. The calculation took into account the optical properties of all components and the CsI quantum efficiency QE(λ) as reported in Ref. [20]. While the measured shape is reproduced by the calculations, the integral photon yield is factor of 1.9 lower than expected. This effect is probably due to a reduced quantum efficiency of CsI. However, the possible aging of the photon converter caused by not yet optimized handling procedures cannot be ruled out and thus no final conclusion can be drawn. Assuming a reduced CsI efficiency and using a C_4F_{10} radiator an average number of $\sim$ 10 detected photons per lepton at small emission angles ($l_{\mathrm{rad}} = 40$ cm) and up to 16 detected photons for larger polar angles can be expected.

The magnetic spectrometer and tracking system

The momentum region of interest ranges from about 200 MeV/c to 1.5 GeV/c. For a two body decays of vector mesons at beam energies of 1–2 AGeV the mean electron momentum varies from 800 MeV/c at a polar angle of 20° to 300 MeV/c at 85°. A mass resolution of the order of the ω-width requires a momentum resolution of $\Delta p/p \leq 1.5\%$ (σ). This requirement can be met using a momentum kick of 50 to 100 MeV/c and a spatial resolution of the coordinate measuring polar angle of each MDC module of ≤ 100 μm (σ) for the geometry chosen.

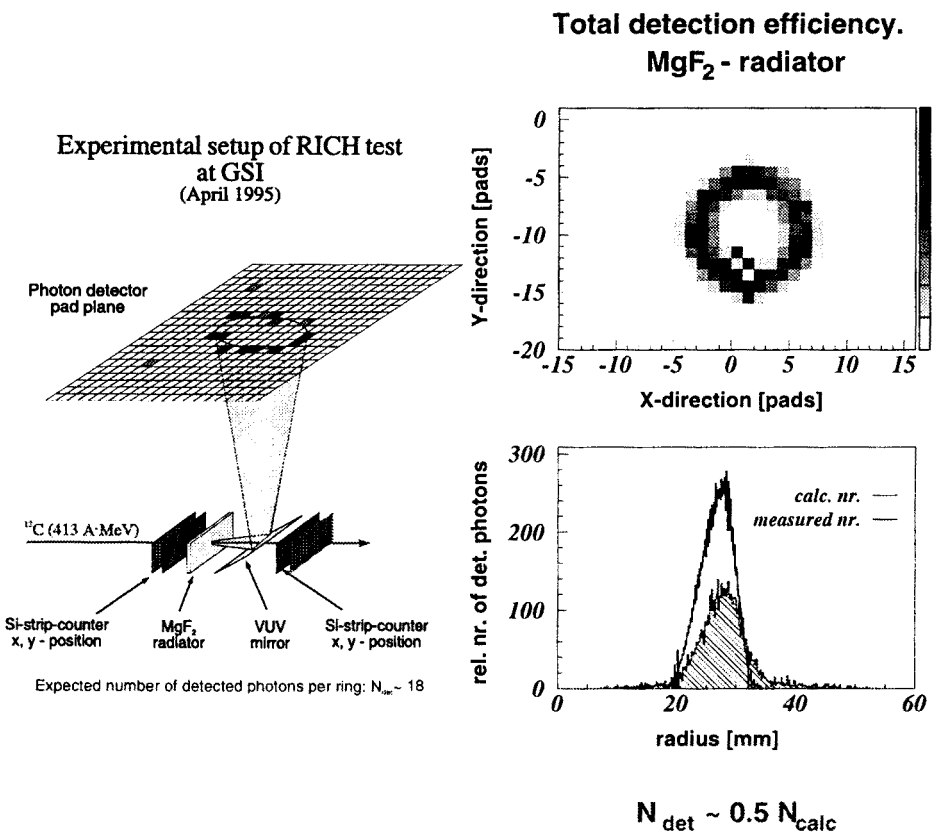

Fig. 5. Test experiment to detect Cherenkov rings produced by $E_{\mathrm{kin}} = 413$ AMeV ^{12}C-ions passing through 2 mm thick Mg_2 radiator. Left figure: Experimental setup to detect Cherenkov rings produced by ^{12}C particles passing a 2 mm thick MgF_2 radiator. Silicon strip detectors are use to derive the ring center position. Right figure: Cherenkov ring obtained after integration over 1700 individual rings. Below, corresponding radial photon distribution in comparison with calculations (hatched area)

The toroidally shaped magnetic field ($B_{\mathrm{max}} = 3.8$ T) will be generated by 6 superconducting coils with individual but interconnected vacuum vessels. Each coil consist of a straight entrance and exit section connected by two arcs (Fig. 1). The total current through a coil amounts to 485 kA turns with 140 turns per coil. The coils have a thickness of 80 mm and consist of a double pancake conductor structure (aluminum stabilized Cu(Nb)Ti 15 × 130 mm^2 each) surrounded by a heat shield at liquid nitrogen temperature and the vacuum chamber. The average current density in the coil

and the total energy stored in the magnetic field is expected be about 120 A/mm^2 and 1.4 MJ, respectively.

Tracking is done outside of the torus with mini-drift chambers, two before and two after the magnetic field region. In order to minimize multiple scattering the volumes in between the MDCs — in particular the magnetic field region — are filled with helium. The charge particle multiplicity in a 1 *A*GeV Au + Au central collision event measured along the polar coordinate and integrated over the one sector amounts to a maximum of 0.6/cm in the innermost MDC. In the outer MDCs the hit density reaches values of 0.22/cm. This number includes, an amount of 15% secondaries produced in the coils and in the inner detectors. To handle this high multiplicity, each module consists of 6 wire planes with a small sense wire spacing ranging from 5 mm (quadratic cells) in the innermost detector to 14 mm (rectangular cells) in the outermost detector. With this wire spacing a double hit probability of less than 0.3 per wire is achieved. The wire tilt angles in the 6 MDC planes vary from -40° to +40° in steps of 20°. The wire positions of the 3rd and 4th plane with 0° tilt angle differ by half a pitch. The choice of these tilt angles ensures an optimal polar angle resolution which is most relevant for a good momentum resolution. It is planned to use 100 μm aluminum field and 25 μm diameter Cu-Be sense wires. To reduce multiple scattering and photon conversion helium based (80% helium and 20% isobutane) counting gas mixture will be used.

The resolution of the tracking system was investigated by the reconstruction of trajectories from simulated leptons events inside the HADES set-up. As an event generator a thermal source (T = 65 MeV, E_{beam} = 1 *A*GeV) of masses between 0.1 GeV/c^2 and 1.2GeV/c^2 decaying into leptons has been used. Fig. 6 shows the mass resolution obtained by the reconstruction algorithm for various position resolution of MDC's. The curve labeled "no multiple scattering" has been obtained switching off this process in the GEANT simulations. The position resolution specified refers to one detector module which consist of 6 planes. At large masses above 0.8 GeV/c^2 the position resolution is the dominant contribution to the mass resolution. Below 0.4 GeV/c^2 , the absolute resolution stays nearly constant, independent of the position resolution. This is due to the multiple scattering inside the target and the RICH radiator and mirror smearing off the lepton opening angle. A relative mass resolution of $\Delta M/M$ = 0.8 % (σ) in the ρ, ω region allows to identify these mesons.

A total of 26828 wires has to be read-out and digitized within 10 μs by electronics placed on the module frames. The analog electronics (preamplifier, discriminator) and TDC will be implemented as independent ASICs. The bit pattern information of the chambers (numbers of fired wires) will be transferred to the third level trigger testing RICH-MDC and

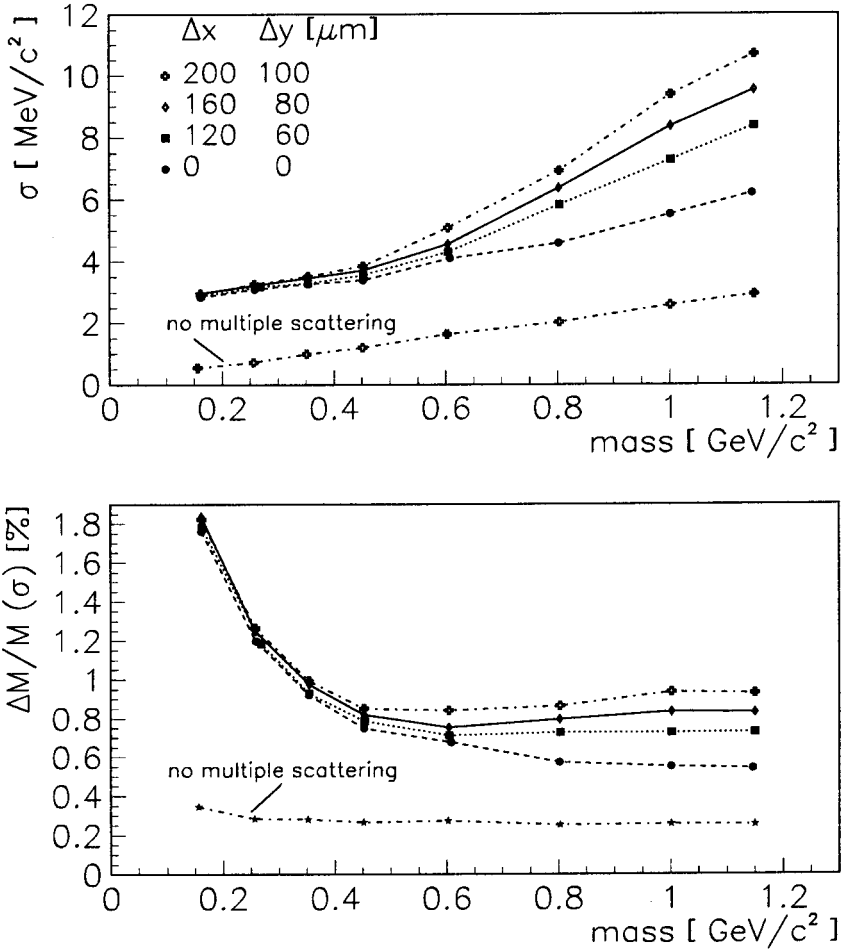

Fig. 6. Calculated absolute(top) and relative (bottom) invariant mass resolution for various position resolutions as a function of the dilepton invariant mass. The solid line indicates designed resolution of the HADES MDC's consisting of 6 separate wire planes. Also shown is the resolution assuming no multiple scattering

META-MDC matching. Drift time values are stored in the local memories and passed to the event builder after positive second level decision, only.

Multiplicity Electron Trigger Array (META)

A fast trigger is crucial to reduce the interaction rate of 10^6/s (for a target with a 1% interaction length and beam intensity of 10^8 particles/s) to a tape event rate of 10^2–10^3/s.

The META is positioned behind the outer MDCs and is designed to provide a first level trigger based on centrality of the collisions as well as a second level electron trigger in conjunction with the RICH.

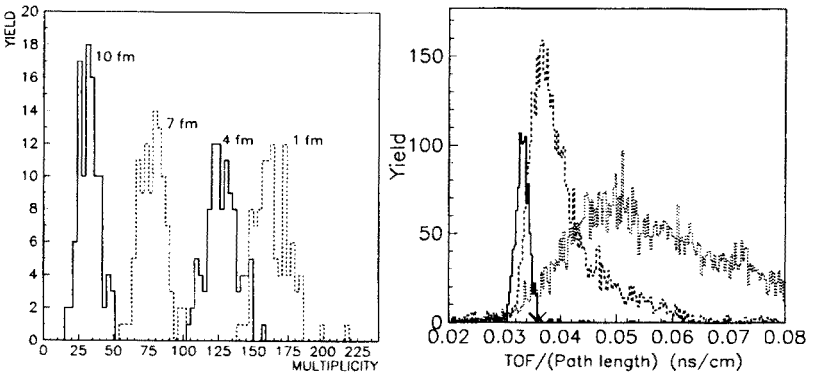

Fig. 7. Expected performance of the HADES TOF system in terms of event characterization (left) and lepton identification(right). Left figure: Expected charge particle multiplicity distribution measured by the TOF system for different impact parameters for 1 AGeV Au + Au collisions. Right figure: Simulated time-of-flight spectra normalized to the target-detector path length for polar angles $> 45°$ for dileptons from ω decay (solid line), pions (dashed line) and protons (doted line) from 1 AGeV Au + Au collisions. The ω dilepton decay has been scaled-up to one decay/per collision

It consist of a TOF wall covering the full HADES acceptance and a pre-shower gas detector system for polar angles $< 45°$. A time of flight wall consisting of scintillator paddles measures the charged particle multiplicity. This allows a selection of central events due to the impact parameter dependence of the particle multiplicity (see Fig. 7) and leads to a reduction of the primary event rate to 10^5/s. The scintillator array consist of 996 strips of rectangular cross section from $40 \times 0.9 \times 0.9$ cm^3 (at 20°) to $227 \times 5.0 \times 3.0$ cm^3 (at 80°). These dimensions have been chosen to limit the multiple hit probability to values smaller than 0.2 in 1 AGeV Au + Au central collisions. Using the time of flight information (resolution of $\Delta t \sim 400$ ps (FWHM) for the shortest paddles has been assumed) for polar angles $> 45°$ a second electron identification is achieved with an efficiency of 96% (Fig. 7). At polar angles $< 45°$ a separation of electrons from pions by time of flight is not possible due to the higher momenta. Here, the electron identification is done with a pre-shower detector positioned behind the scintillator strips. One sector of the pre-shower detector consists of a stack of three wire detectors and two Pb-layers (two radiation lengths each) in between (Fig. 8).

The gas chambers operate in self-quenching streamer mode (SQS), where the produced charge is nearly independent of the particle energy loss and depends only on the number of charged particles measured in the chamber. The counters are filled with an argon/isobutane/hepthane (0.32 : 0.64 : 0.04) mixture and have only one wire plane with 7.5 mm sense wire (25 μm golded tungsten) to field wire (125 μm Cu-Be) spacing and a 4 mm cathode to wire plane separation. The induced charge is read on the cathode plane divided into 32 x 32 copper pads of varying dimensions (from 1.5 x 3 cm^2 at small polar to 5 x 4.5 cm^2 at large polar angles). The pads are organized in rows and columns and aligned in each sector with respect to the target, such that there is a one-to-one correspondence between a pad in a particular row and column in all 3 detectors. The lepton identification is performed by means of comparison of the integrated charge on the preshower (before the lead converter) and two post shower (after the lead converters) detectors. Dedicated GEANT simulations show that maximum shower detection efficiency can be obtained by integrating the charge inside a radius of $R \sim 4.5$ cm around the shower axis, corresponding to an area of ~ 9 pads for 1.1 cm converter-gas chamber distance. The pre-shower detector single lepton efficiency ranges from 60% for an electron momentum of 300 MeV/c to about 90% at 800 MeV/c. The chambers have to operate stable for a high charge particle counting rates of up to 200 particles/cm^2s in the Au+Au central collisions at 1AGeV. Misidentification of hadrons by META (TOF and Pre-shower) results in $\simeq$ 8 fake electron candidates per collision.

A total of 18432 pads will be read-out by connecting each row of one gas chamber to one analog ASIC, designed in Krakow. The chip, similarly to AMPLEX , consists of a charge preamplifier, shaper and sampler hold stage triggered by an external signal but will have much higher dynamic range (up to 60 pC input charge) and 32 channels. Each row is read-out in parallel into individual 8 bit flash-ADC and the digitized data are send to a shower recognition trigger processor based on FPGA. In contrast to the RICH processor, the shower processor works with the analog information (8bit instead of 1 bit pad-hit pattern) and thus has to process more data. However, the general readout scheme will also be adopted here. The zero suppressed data will be stored in the local memories until the second level trigger decision takes place. Then they will be transferred to the event builder or will be discarded depending on the second level trigger decision.

The pre-shower detector prototype performance

Two prototype chambers of 40 x 40 cm^2 have been constructed. In the first tests the second cathode plane was build from Al coated MYLAR foil. With the designed gas mixture the SQS mode has been achieved at about

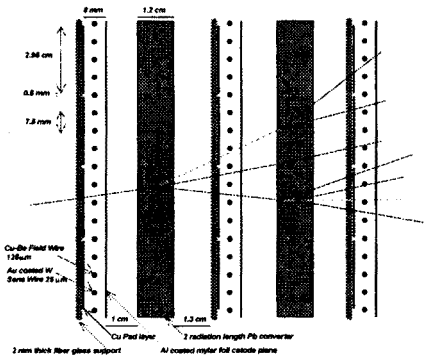

Fig. 8. Schematical side view of the pre-shower detector. A stack of 3 gas chambers and two Pb-converters are positioned at polar angles $< 45^0$ behind the TOF wall. The chambers operate in self-quenching streamer mode. The induced charge is read-out from pads covering the cathode plane

3.2 kV. The plateau for this chamber had 350 V width, followed by a high current leap.

The tests was performed with β particles from a ^{90}Sr collimated source. Observed were ~30 mV signals on 50 Ohms with a rise time 3 ns and fall time of 20 ns corresponding to $\sim$ 5pC charge collected on the pad. The chamber could handle $\sim$ 200 particles/mm^2/s. Shown in Fig. 9 (left) is the induced charge on the struck and 8 surrounding pads from a Sr β particles.

However, for larger electron intensities self propagating signals even after removing the source were observed. We concluded that this effect was due to secondary electrons from the photoelectrical effect on the Al cathode foil (due to the small photon energy threshold for photoeffect in aluminum). To improve the situation the cathode foil was replaced by a multiwire cathode plane with 2mm (125 μ diameter Cu-Be) wire spacing. As a result, the chamber operates stable with much higher counting rates without the appearance of the self-counting mode. The test for shower detection has been performed at the MAMI electron accelerator in Mainz. A continous electron beam of 850 MeV and $\sim$ 2000 particles/mm^2/s was impinging on the gas chambers (pre and post-shower) separated by a 2 radiation length of Pb converter. Data acquisition was triggered by a coincidence of two 2mm diameter scintillating fibers crossed in front of the central pad. In Fig. 9 (right) the charge distributions integrated over 9 pads (8 pads surrounding

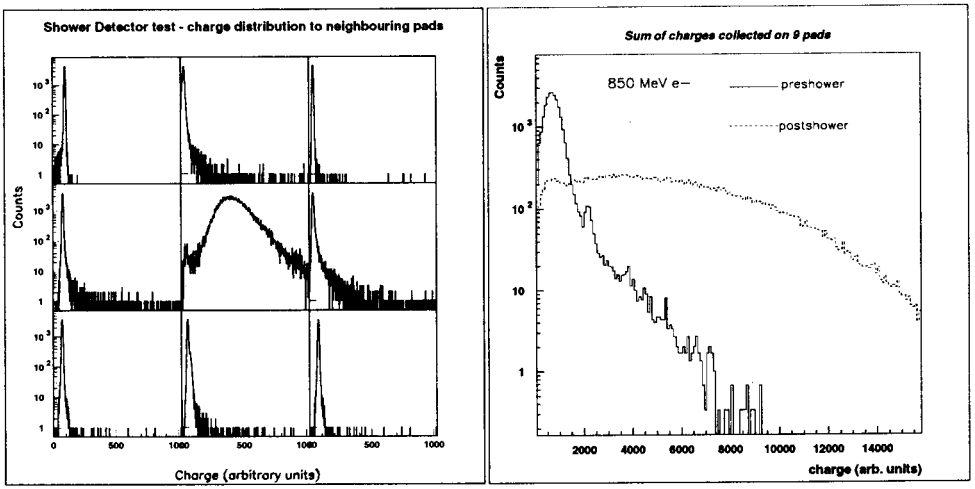

Fig. 9. Results obtained from the test of the HADES prototypes of SQS chambers of the META detector performed with radioactive sources (left) and a 850 MeV electron beam (right). Left figure: Measured induced charge distributions on 9 neighbouring pads. A collimated β Sr source was placed in front of the central pad. The prominent peak in the central pad charge distribution indicates SQS mode. In agreement with calculations, neighbouring pads see only little charge. Right figure: Electromagnetic shower from 850 MeV electrons detected in the prototype of the META preshower detector. Intergrated over 9 pads the charge distributions are compared for the preshower(solid line) and post shower (dashed lines) positioned behind a 2 radiation length Pb converter.

central struck pad) in the preshower (solid line) and post shower (dashed line) for a 1.1 cm post-shower-lead converter distance are presented. The comparison of these two integrated charge values is the idea behind the shower recognition algorithm. When assuming a charge threshold of 1200 (arbitrary units of Fig. 9) a $\sim$84% single electron shower detection efficiency can be derived from the measured data. This value is in good agreement with the simulated value from the GEANT code.

Performance simulation

The performance of the spectrometer has been studied using GEANT simulations including the detailed HADES geometry, realistic detector response and calculated field map. As a most difficult scenario 1 AGeV central Au + Au collisions were investigated. The event generators were taken from BUU and IQMD/RQMD calculations [22, 25]. Simulated events were analyzed by a dedicated analysis program. In the first stage of the algorithm

central events were selected and investigated by the second level trigger condition. As it has already been mentioned above, the second level trigger is based on the spatial matching of recognized electron candidates both in the RICH and the META detector. Fig. 10 (a) shows the second level trigger efficiency normalized to the the HADES geometrical acceptance (~40% at midrapidity $Y = 0.65$–0.8) (left) for pairs from a thermal source with $T = 65$ MeV and $T = 95$ MeV. The trigger efficiency is mainly determined by the META detector system efficiency (in particular a loss of shower efficiency at low momenta) and by the RICH META angular matching window. For the latter, strong bending of the lepton trajectories at small momenta results in a loss of efficiency. Requiring a background reduction factor of 100 for central 1 AGeV Au + Au collisions results in a matching window of $\Delta\Theta$=20°.

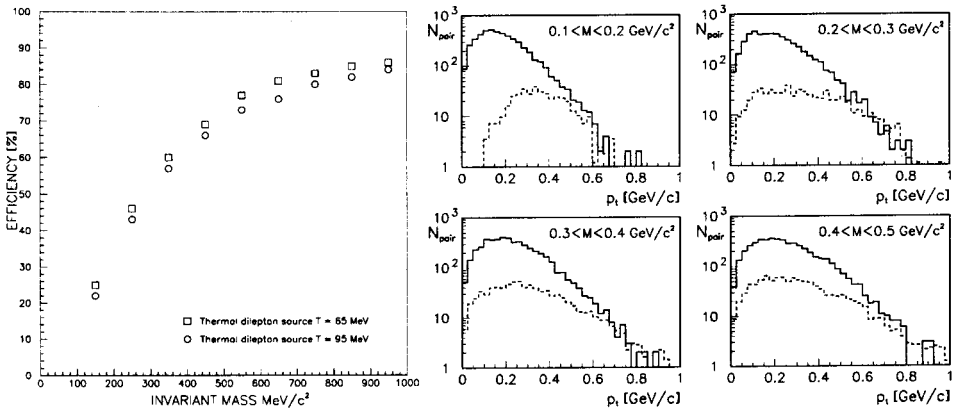

Fig. 10. Simulated HADES detection trigger efficiency (left) and total detection efficiency (right). Left figure: Second level trigger efficiency normalized to the geometrical acceptance (~40%) as a function of dilepton invariant mass. The trigger checks a condition on angular matching of hits recognized as an electron, both in the RICH and, in the META detector. Right figure: Tranferse momentum distribution of reconstructed pairs emitted from a thermal source ($T = 65$ MeV) (dashed lines) for different invariant mass regions. The primary distributions (solid lines) are also shown for comparison. The detection efficiency includes: geometrical acceptance,second level trigger and reconstruction efficiencies

In the next stage, a track reconstruction form MDC hits and track fitting was performed for triggered events. The total reconstruction efficiency as a function of invariant mass is nearly mass independent and amounts to about ~65%. As a example of the final result transverse momenta distribution for dielectrons from a uniform mass distribution emitted by a thermal

source are presented in Fig. 10 (b). The decrease of detection efficiency at small p_t and small invariant masses is caused by trigger efficiency losses. However, this decrease of efficiences at small masses and small p_t is compensated by larger dielectron production cross section at low invariant masses.

Extraction of the dielectron signal

After track reconstruction the remaining background consists of uncorrelated e^+ and e^- tracks originating from Dalitz decay processes ($\pi^0 \rightarrow \gamma e^+ e^-$) or external conversions ($\gamma \rightarrow e^+ e^-$) in the RICH radiator or target material. These tracks originate mostly from a close pair resulting in close RICH rings which cannot be resolved. However, both tracks of the one pair are detected in the inner MDCs but mostly one of the electrons gets later lost by the strong deflection in the field region. Therefore, a powerful rejection method is a search for the typical hitpattern of close tracks in the inner MDCs connected to only one RICH ring. Rejecting close tracks reduces the background by an order of magnitude to the final amount shown in Fig. 11(a).

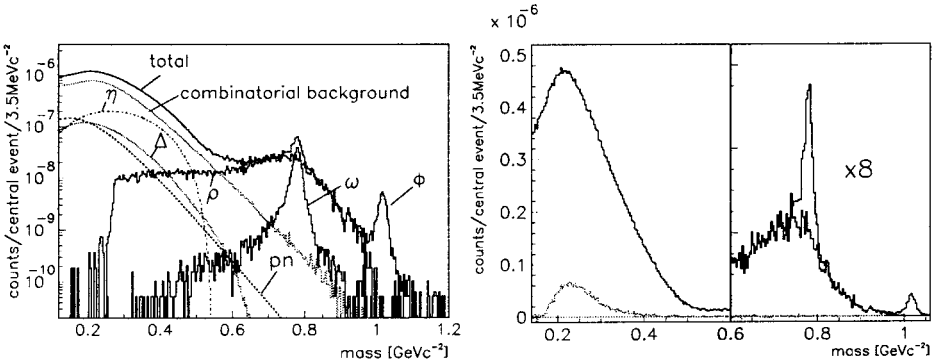

Fig. 11. Invariant mass spectrum for the main e^+e^- sources for 1 AGeV Au + Au collisions. Left figure: Individual contributions to the total dielectron mass yield. Dalitz decay of η and Δ and pn-bremsstrahlung are the main contributing sources below 0.5 GeV/c^2. Above 0.5 GeV/c^2 dielectrons from ρ, ω and ϕ mesons dominate the spectrum. Right figure: Same as left after subtraction of the background obtained from like sign pairs. The remaining background contribution is shown separately (dotted histogram). Note the different scale for masses > 0.6 GeV/c^2.

The different contributions to the reconstructed invariant mass spectrum in Fig. 11 (a) are taken from theoretical models [1, 2]. The cross sections are consistent with experimental data [9]. For the ϕ meson the cross section is estimated based on a preliminary calculation of Ko [3]. Above

600 MeV/c^2 the contributions of ρ, ω and ϕ clearly dominate the spectrum. Fig. 11 (b) shows the reconstructed invariant mass spectrum after subtraction of combinatorial background derived from like sign pairs. The signal from Dalitz decays of Δ's and η's as well as from *pn*-bremsstrahlung is clearly visible below 500 MeV/c^2. The dotted line shows the residual background resulting from the different spectrometer acceptance for like and unlike sign pairs.

Conclusions and prospects

With a high count rate capability and a high geometrical acceptance HADES will be able to measure e^+e^- pairs for the heaviest systems and highest SIS energies. With an invariant mass resolution of better than 1%(σ) a clear identification of ω, and ϕ, ρ can be achieved. The reduction of combinatorial background by rejecting close tracks results in a signal to background ratio of 10:1 in the ρ/ω region (Fig. 11 (b)) for the most difficult case of 1 *A*GeV Au + Au collisions.

It has been shown that HADES is an ideal detector to study in-medium modifications of meson masses. With the anticipated mass resolution it will be possible to find or rule out a mass shift of mesons decaying inside dense hadronic matter. Moreover, it will be possible to study this effect as a function of nuclear density. As a tool to such an experiment the narrow ω or ϕ mesons can be used. Although they have long life-times (*i.e.* ω life time is 23 fm/c) and mostly decay outside of the collision zone one can use the method of recoilless production to trigger on decays inside the nucleus. Such an experiment could be done using a pion beam impinging on heavy nucleus. The anticipated reaction is $\pi^- p \rightarrow \omega n$. The proper kinematical condition is achieved if the omega momentum points backwards and is high enough to compensate the CM velocity in the laboratory frame. Such condition could be tagged by forward detection of the recoiling neutron i.e by combined HADES and GSI neutron detector LAND [27] or a trigger on e^+e^- pairs showing a large opening angle. Another important topic, discussed in the Soyeur contribution, which can be address by HADES physics program are hadron and meson form factors. For example the time-like formfactor of vector mesons are not fully described by the Vector Dominance Model in the case, where the vector meson is transformed into another meson (ω meson formfactor [26]). An appropriate experiment would again exploit pion induced omega production. Combination of HADES and an electromagnetic calorimeter would permit omega and dielepton invariant mass ($\omega \rightarrow \pi^0 e^+ e^-$) reconstruction and thus permit form factor measurement.

This work has been supported in part by the Bundesministerium für

Forschung und Technologie of the Federal Republic of Germany under contracts No: GI475ITEP4, OF474TP4, TM353TP6 Human Capital and Mobility Program and Polish-German Fundation: Stiftung Deutsch-Polnische Zusammenarbeit, Fundacja Współpracy Polsko Niemieckiej under contract 528/92/LM. We would also like to thank very much prof. H. Harrah group at the Mainz University for allowing us use their test beam times and facilities for the experiment with the HADES preshower-detector prototype.

REFERENCES

[1] L. Winckelmann, NATO Advanced Study, Bodrum 1993.
[2] Gy. Wolf, W. Cassing, U. Mosel, *Nucl. Phys.* **A552**, 549 (1993).
[3] C.-M. Ko, Workshop on Dilepton Production in Relativistic HI Collisions, Darmstadt(GSI) 1994.
[4] M. Herrmann, B. Frimann, W. Nörenberg, *Nucl. Phys.* **A545**, 267 (1992).
[5] G. Chanfray, P. Schuck, *Nucl. Phys.* **A489**, 271 (1992).
[6] G.E. Brown, M. Rho, *Phys. Rev. Lett.* **66**, 2720 (1991).
[7] T. Hatsuda, S.H. Lee, *Phys. Rev.* **C46**, R34 (1992).
[8] M. Asakawa, C.M. Ko, *Phys. Rev.* **C48**, R526 (1993).
[9] V. Metag, *Prog. Part. Nucl. Phys.* **30**, 75 (1993).
[10] A. Yegneswaran *et al.*, *Nucl.Instrum. Methods Phys. Res.* **A290**, 61 (1990).
[11] D. Miskowiec *et al.*, *Phys. Rev. Lett.* **72**, 3650 (1994).
[12] High energy collisions GSI Report GSI-87-10 ISSN 0171-4546 1987 eds H. Gutbrod, A. Sandoval, R. Stock.
[13] A. Dress *et al.*, Proceedings of the International Workshop XXIII on Gross Properties of Nuclei and Nuclear Exitations, ed. by H. Feldmeier 1995, p. 151.
[14] C. Naudet *et al.*, *Phys. Rev. Lett.* **62**, 2652 (1989).
[15] HADES Letter of Intent, Dec 1991, HADES Design Study, Nov 1992.
[16] HADES, GSI Scientific reports 1992 (379-383), 1993.
[17] HADES, Proposal for High-Acceptance Di-Electron Spectrometer, 1994.
[18] R. Gernhaeuser *et al.*, RICH 95 conference, Uppsala to be published in *Nucl. Instrum. Methods Phys. Res.*
[19] E. Beuville *et al.*, *Nucl. Instrum. Methods Phys.Res.* **A288**, 157 (1990).
[20] H. Berger *et al.*, *Nucl. Instrum. Methods Phys. Res.* **A360**, 411 (1995).
[21] J. Carrol, *Nucl. Phys.* **A495**, 409c (1989); H.Z. Huang *et al.*, *Phys. Rev.* **C49**, 314 (1994).
[22] Gy. Wolf, W.Cassing, U. Mosel, *Nucl. Phys.* **A552**, 549 (1993); Gy. Wolf private communications.
[23] S.C. Joeng *et al.*, *Phys. Rev. Lett.* **72,22**, 3468 (1994).
[24] V. Metag *Prog. Part. Nucl. Phys.* **30**, 75 (1993).
[25] L.A Winkelmann *et al.*, *Phys. Lett.* **B298**, 22 (1993); L.A. Winkelmann, S. Bass private communications.
[26] L.G. Landsberg, *Phys. Rep.* **128,6**, 301 (1985).
[27] Th. Blaich *et al.*, *Nucl. Instr. Meth.* **A314**, 136 (1992).